Heliyon 10 (2024) e26788

Contents lists available at ScienceDirect

Heliyon

journal homepage: www.cell.com/heliyon

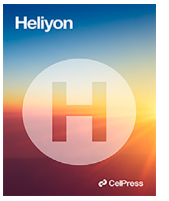

Research article

The energy park of the future: Modelling the combination of wave-, wind- and solar energy in offshore multi-source parks

Hinne F. van der Zant, Anne-Caroline Pillet, Anton Schaap, Simon J. Stark, Timothy A. de Weijer, Aida A. Cahyaningwidi, Benjamin A.E. Lehner *

ARTICLE INFO

Keywords:
Renewable energy
Wave energy
Wave energy converter
Floating solar
Offshore PV
Photovoltaics
Offshore wind
Multi-source
Co-location
Baseload
Grid balancing

ABSTRACT

To mitigate the effects of climate change, a significant percentage of future energy generation is set to come from renewable energy sources. This has led to a substantial increase of installed offshore wind in the North Sea in the last years (28 GW in 2021) and is projected to further accelerate to an installed capacity of 212 GW by 2050. Increasing the renewable energy grid penetration brings challenges, including 1) limitations in space availability and 2) the reliability of renewable energy systems in terms of grid balancing. In the North Sea, maritime space is getting scarce and the projected upscaling of offshore wind is putting pressure on the chemical-, biological, and physical balance of the marine ecosystem. Without economically viable large-scale storage systems, a renewable energy system focused on one intermittent source does not provide reliable baseload- and energy demand compliance. By integrating different supplementary offshore renewable energy sources into multi-source parks output becomes smoother, while the energy yield per area increases. Despite multiple studies stating the benefits of multi-source energy parks of either wind and wave energy or wind and PV energy, no study has been conducted on the co-location of all three offshore renewables. This study combines and analyzes the three offshore renewable energy sources: wave-, offshore PV- and wind energy in the example of Ten Noorden van de Waddeneilanden, a future wind farm north of the Dutch Wadden Islands. The additional renewables are allocated within the wind turbine spacing, taking into account safety zones and maintenance corridors. Co-location of these renewables increases the extracted energy density by 22%, making more efficient use of the limited available marine space. Moreover, the park output becomes smoother as the yearly-averaged coefficient of variation decreases by 13%, the capacity factor with respect to the export cable increases by 19%, and the hours where the output of the park is below 20% of the export cable capacity decreases by 86.5%.

1. Introduction

While fossil fuels are finite resources and their combustion emits harmful greenhouse gasses, renewable energy technologies offer a sustainable and renewable alternative. Many countries are therefore planning to strongly increase renewable energy build-out. For example, a minimum of 45% of the energy generation in the European Union is set to come from renewable energy sources by 2030 [1]. Favourable bathymetry and wind resource availability, paired with close proximity to large energy consumers have

* Corresponding author.
E-mail address: benjamin@dutchmarineenergy.com (B.A.E. Lehner).

https://doi.org/10.1016/j.heliyon.2024.e26788
Received 29 June 2023; Received in revised form 19 January 2024; Accepted 20 February 2024

Available online 28 February 2024

Nomenclature

WECs	Wave Energy Converters	CF	Capacity Factor
PV	Photovoltaics	KNMI	Royal Netherlands Meteorological Institute
TNW	Ten Noorden van de Waddeneilanden, a future Dutch offshore wind farm	SWAN	Simulating WAves Nearshore
PCC	Pearson Correlation Coefficient	PVGIS	Photovoltaic Geographical Information System
CoV	Coefficient of Variation	PCC	Pearson Correlation Coefficient

made the North Sea a global hotspot for offshore wind energy production [2–4]. In 2021, 28 GW of offshore wind were installed in the North Sea [5] and a substantial increase is planned to 212 GW by 2050 [6][4]. Installing this amount of offshore wind in the North Sea has raised concerns about numerous physical, chemical and biological impacts [2,4,7–14]. The physical potential related to kinetic energy replenishment from higher atmospheric layers is estimated to be 2 MW/km^2[2] and a sustainable installed power density for wind farms is determined to be 2-4 MW/km^2[2,15], assuming sufficient spacing between the wind farms. However, the average installed energy density of wind farms in the North Sea is approximately 7 MW/km^2 and thus most existing wind farms are generating electricity in an unsustainable manner [2]. Therefore, continuing to build wind farms at current energy density results in the loss of offshore wind energy resources and ultimately loss of revenue. Furthermore, without economically viable large-scale storage systems, a renewable energy system dominated by one intermittent source is not reliable in terms of grid balancing [16,17] as it relies on the need for non-renewable backup plants. Offshore multi-source parks increase the energy density, making more efficient use of the available marine space and while there is a high potential for more reliable output, no quantified research on park levels exists yet.

The concept of combining wave- and wind energy was proposed as early as 2010 by [18] and [19], and in more recent years, the benefits have been explored in various publications. By integrating different offshore renewable energy sources, the park output as a whole can become smoother, as the timing at which each source produces power can be complementary, for both wave-wind [20–23] and offshore PV-wind [24,25] combinations. At the same time, multi-source parks of either wave-wind or PV-wind can increase the extractable energy density of the park reducing the overall space requirements [26–29]. The spacing between offshore wind turbines can be used to accommodate these supplementary offshore renewable energy technologies. Incorporating different marine energy technologies at one location can further reduce the relative project costs by sharing the offshore grid infrastructure [30,31] and increase the accessibility for operation and maintenance (O&M) to wind turbines due to wave height reduction [32,33]. Synergies associated with wind-wave parks, which include enhanced power predictability and smoothness, as well as milder in-park wave climates, have been described in [32,34,35]. The positive findings of combining wave- and wind energy lead to multiple studies proposing the optimal layout for co-location of wave and wind energy [21,36–42]. However, to the best of the authors' knowledge, no research has been conducted on the multi-source offshore energy park combining wave-, offshore wind- and offshore PV.

To quantify this potential, a five-year-long time-series analysis has been performed on the available wave-, wind- and PV energy resources at Ten Noorden van de Waddeneilanden (TNW), a wind farm north of the Dutch Wadden Islands (54.036111°N, 5.963056°E). This location was chosen because of its auspicious wave energy potential and the planned development time for the project matches well with the anticipated demonstration and commercialization timelines for wave energy and offshore PV. In some regions of the North Sea, the expected yearly mean of wave energy available for harvesting is ~15 kW/m, showing seasonality variability with the highest values in winter and lowest in summer [26,43]. In upper North Sea latitudes, wave resources are more energetic, reaching >30 kW/m in deep waters [43]. This paper contributes to marine energy research by proposing and providing first-order quantification of a novel concept that is becoming increasingly relevant for the offshore energy sector and not yet realized in the market.

2. Methods

2.0.1. Spatial park design

To assess the potential of a multi-source ocean energy project at TNW, a spatial design is needed to extrapolate the available offshore resources to a large-scale park. The boundaries of the proposed TNW wind farm site are based on a report by BLIX Consultancy and partners [44], taking into account the wake effect of the adjacent existing wind farm Gemini. The wind turbine spacing is optimized, such that internal wake effects and the required length of inter-array cables are minimized inside the proposed periphery of the park [44]. Legally required exclusion zones have been considered; a 500 m radius around wind turbines and 250 m on each side of the cables based on a study by Pondera for a multi-source park design of the wind farm Borssele [45]. In this study, the additional offshore renewable energy sources are allocated within the proposed spatial park design, taking into account the safety zones- and maintenance corridors of the offshore wind turbines. The rationale is that the first multi-source energy projects are likely to be added to existing wind farms and therefore do not have an optimized layout for maximizing the business case for all installed renewable energy sources.

For TNW, 63 wind turbines are planned with a rated capacity of 12 MW each [44]. The transmission system operator of the Netherlands, TenneT, is planning to utilize 66 kV inter-array cables, which can transport 80 MW [46] towards the offshore substation.

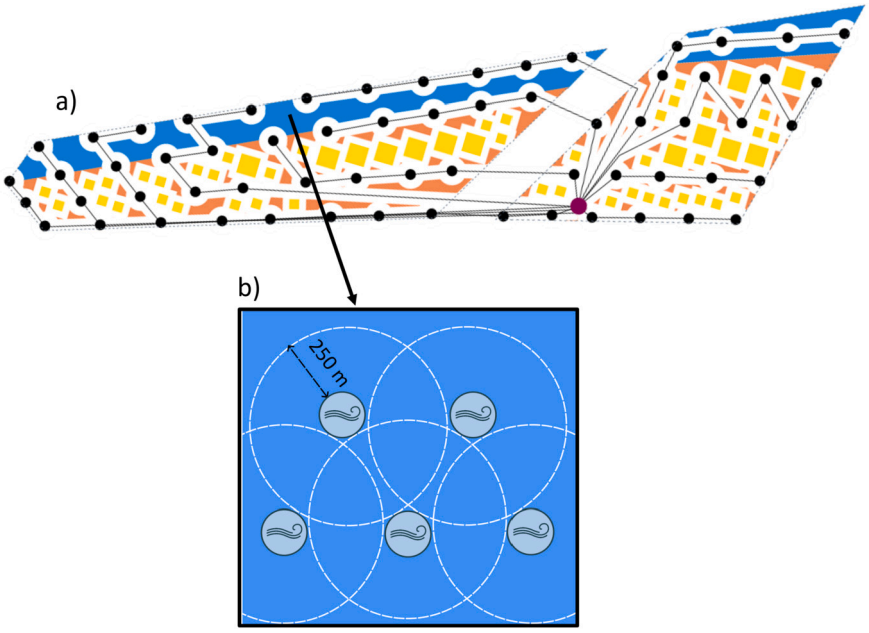

Fig. 1. a) Proposed spatial design for TNW with integrated offshore PV systems with a size of 250 m x 250 m and 500 m x 500 m. Black dots indicate the locations of wind turbines, black lines are inter-array cables and the yellow squares are PV systems, surrounded by white areas that depict the legally required exclusion zones. The purple dot is the offshore substation. The blue area is designated to capture wave power. b) Proposed WECs configuration, based on tests by Deltares performed on the SlowMill wave energy converter [51].

This would imply that 6 to 7 of 12 MW rated wind turbines with a total capacity of 72-84 MW can be accommodated per inter-array cable.

The proposed wind farm design of TNW was made in scale in Inkscape, an open-source scalable vector graphics editor, allowing for accurately scaled drawings [47]. Fig. 1 depicts the scaled multi-source spatial park design of TNW that is used in this paper. Accounting for wind turbines, maintenance corridors, and inter-array cables and their respective exclusion zones, offshore PV installations of 250 m by 250 m and 500 m by 500 m have been placed within the available spacing. Exclusion zones of 250 m surrounding the PV installations have been considered, allowing for a total installed PV capture area of ~5.8 km^2 (~ 5% of the total area). The blue area in Fig. 1a, following the north/north-west perimeter of the park, corresponding to the prevailing direction of the incoming wave field [48], is designated for Wave Energy Converters (WECs). This will be further referred to as the active perimeter and is estimated to be ~19.75 km, based on the scaling of the proposed park outline [49,50]. Scaled tests performed by Deltares [51], suggest that a staggered configuration is optimal for wave energy absorption while minimizing the number of WECs required, potentially lowering the initial investment costs. In this staggered setup, the WECs are placed in a 60°- 60°- 60° configuration and this paper considers a conservative spacing of 250 m for safety requirements related to mooring and range of movement, as depicted in Fig. 1b. The number of WECs in a row with a staggered setup for a certain unit of length is approximated as:

$$N_{WECs} = 1.5 \times \frac{L+S}{B+S} \tag{1}$$

Where, N_{WECs} is the number of WECs, L [m] is the length along which the WECs are placed. S is the spacing between the WECs and B [m] is the length of the WEC. The WEC considered in this study is the 600 kW Wavestar, which is designed for the wave climate in the North Sea. WaveStar has 20 floaters with a diameter of 6 meters each that capture the wave energy and the total length of the device is 70 meters [52]. Based on Equation (1), the number of wave energy converters (N_{WECs}) that can be accommodated in the active perimeter is 94.

2.1. Power modelling

2.1.1. Wave energy

In 2009, a prototype WaveStar of 600 kW was installed and produced output from May 2010 to December 2012 on the Western coast of Denmark [52]. The results of this demonstration have been used to validate the power matrix of the WEC (Table 1), which describes the generated electric power as a function of significant wave height (H_s) and peak wave period (T) [53]. Below $H_s < 0.5$ m and for all T, there is not enough energy in the waves for the device to generate electricity. Above $H_s > 3.0$ m, the device goes into storm protection mode and no longer produces output. The datasets H_s and T are obtained from the output of SWAN (Simulating WAves Nearshore), developed by Delft University of Technology (TU Delft). SWAN is a third-generation wave model that estimates wave conditions in open oceans and coastal regions for given wind and bathymetry conditions, by solving the action density balance

Table 1
Wavestar prototype electrical power matrix in kW. Originally published by Wavestar, adopted from [59].

Wave height H (m)	Wave period (s)										
	2 – 3	3 – 4	4 – 5	5 – 6	6 – 7	7 – 8	8 – 9	9 – 10	10 – 11	11 – 12	12 – 13
0.0-0.5	0	0	0	0	0	0	0	0	0	0	0
0.5-1.0	0	49	73	85	86	83	78	72	67	63	59
1.0-1.5	54	136	193	205	196	182	167	153	142	132	123
1.5-2.0	106	265	347	347	322	294	265	244	224	207	193
2.0-2.5	175	429	522	499	457	412	372	337	312	288	267
2.5-3.0	267	600	600	600	600	540	484	442	399	367	340
3.0-	Storm protection										

for numerous physical processes explicitly [54–56]. The modelled SWAN wave data shows good agreement with observations and provides a longer and unfragmented time series, compared to most measurement campaigns [56,57]. For the TNW region, SWAN simulates a yearly average wave energy of 15.22 kW/m for TNW, agreeing with North Sea wave energy resources described in literature [58]. Based on this average wave energy availability, the resulting capacity factor (CF) for the WaveStar in the modelled example is 36.4%.

2.1.2. PV energy

The power generation by PV cells is quantified with the following formula:

$$P_{PV} = A \times eff \times H \times PR \tag{2}$$

Where, P_{PV} [W] is the generated power by the PV cell, A [m^2] the PV capture area, eff [-] the PV efficiency, H [W/m^2] the incoming solar irradiance, and PR [-] the performance ratio; a coefficient that accounts for losses, such as degradation fouling and inverter losses. For this study, an efficiency of 20% and a PR of 0.77 is considered [60]. The irradiance database used as input is satellite data from the PVGIS-SARAH2 satellite, with a resolution of 0.05°x 0.05°, processed by PVGIS [61]. PVGIS does not provide irradiance data of the ocean and therefore the solar data from Ameland (53.468° N, 5.958° E) is used as input, as it is closest to TNW. PVGIS provides an hourly irradiance dataset of the chosen location, correcting for an optimized slope- and azimuth angle for the PV system. As such, the PVGIS dataset can directly be used to compute P_{PV}.

2.1.3. Wind energy

The wind energy of the multi-source park is approximated as:

$$P_{wind} = N_{turb} \times \frac{1}{2} A \rho v^3 \times C_P \times eff_{park} \tag{3}$$

Where P_{wind} [kW] is the power generated by the wind turbine. N_{turb} is the number of wind turbines in the park, A [m^2] is the rotor area which is set to 220 m, based on the General Electric Haliade-X 12 MW offshore wind turbine [62]. ρ [kg/m^3] is the density of the air, v [m/s] is the wind speed at hub height and C_p [-] is the power coefficient, representing the efficiency of the wind turbine. Due to the tip vortices of the wind turbines, as well as the pressure drop over the rotor plane, the turbulence in the wake of each in-farm turbine is increased and the wind speed is reduced. The model corrects for the wake effect with the imposed eff_{park} [-] factor. Wind speed data sets are downloaded from the Royal Netherlands Meteorological Institute (KNMI). Hourly KNMI measurements from the offshore L9 platform (53.61384° N, 4.96089° E), which is located ~80 km west of TNW are used [63]. The wind speed is measured at 10 m height, so a correction factor is applied to account for the increasing vertical velocity profile of wind, based on the logarithmic wind profile for low surface roughness ($z_o = O \approx 10^{-4}$) [64,65]. The cut-in speed is set to 4 m/s, the rated wind speed is 12 m/s and the cut-out wind speed is 25 m/s [66]. In the studied time range, there are 151 data gaps in the hourly wind speed data set (0.3% of the analyzed hours). To minimize data gaps, the data set has been linearly interpolated with a limit of 48 consecutive hours. This limit is imposed, such that data gaps (>48 hours) are not interpolated, as large interpolations impose unrealistic data manipulation and potentially fallaciously influence the, especially statistical, analysis of this study.

2.2. Parameterizing reliability and smoothness

2.2.1. Complementarity

The complementarity of renewable energies is one of the most important aspects of feasibility studies on multi-source marine energy projects [67]. Offshore renewables strongly depend on environmental resources, which do not always align with timely energy demand. As a measure for complementarity in the multi-source study of TNW, the yearly- and seasonal Pearson Correlation Coefficient (PCC) has been established for different time series frequencies. The PCC is used, as it is statistically more robust than other well-known non-parametric correlation coefficients such as Kendall- and Spearman correlation coefficient, which tends to neglect fine information included in the data sample [67]. However, a disadvantage of using PCC is that it is not appropriate for variables that share a nonlinear relationship, unlike the above-mentioned alternatives [67]. To determine the degree of linearity

between the considered offshore renewables, both the Kendall- and the PCC have been computed. If both coefficients are similar, it can be assumed that the two input variables share a linear relation. In Appendix A, the Kendall correlation coefficients are shown. The PCC is defined as [67]:

$$r(X,Y) = \frac{cov(X,Y)}{\sigma_X \sigma_Y} \tag{4}$$

Where X and Y correspond to one of the considered offshore correlation renewables, $\sigma_{X,Y}$ is the standard deviation, and $cov(X,Y)$ is their covariance. Positive values denote a correlation between the two variables implying that if one variable is increasing (decreasing), the other is also increasing (decreasing). A negative sign indicates an anti-correlation and suggests opposite behavior. The association between the variables becomes weaker as the value of the correlation coefficient approaches 0. Ideally, the considered offshore renewable energy sources share an anti-correlation, such that when there is no wind, there can still be park output impending from wave- and/or PV power. For a hybrid energy assessment, negative values indicate complementarity and positive values suggest synergy [67]. Correlation coefficient in the interval (|0.3|, 0.0) suggests weak correlation, (|0.6|, |0.3|) moderate correlation, (|0.9|, |0.6|) strong correlation and (|1.0|, |0.9|) very strong correlation [68]. The PCC has been determined on a seasonal and yearly timescale, to determine the seasonal variability in complementarity. Moreover, this analysis has been performed for three different time series frequencies (hourly, daily, and weekly) to filter out certain signals in the input variables. For example, any correlation with offshore PV using an hourly sampled data set will return a coefficient close to 0, due to the day-night cycle. By increasing the time series frequency, for example, to daily, the signal of the day-night cycle becomes less apparent in the correlation coefficient, see Appendix B.

2.2.2. Smoothness

The smoothness of the multi-source offshore farm is determined by computing the coefficient of variation of the farm output:

$$CoV = \frac{STD}{Mean} \tag{5}$$

Where STD is the Standard Deviation of the power output of the farm and $Mean$ is the average farm output. Smaller values for CoV imply that the standard deviation relative to the mean is small and therefore there is not a lot of timely variation in the output.

2.2.3. Capacity factor

The Capacity Factor is a measure of how much electricity is generated on average over a period of time compared to its maximum potential. Note that in this study, we present the CF with respect to the export cable, which can be interpreted as how much electricity is generated over a period of time in relation to the size of the export cable. In this context, the CF is defined as:

$$CF = \frac{Actual\ Energy\ Output}{Export\ Cable} \times 100 \tag{6}$$

Where CF is the Capacity Factor in %, Actual Energy Output is the total amount of electrical energy generated in the park in a certain period of time [GWh] and Export Cable is the amount of electrical energy that can be transported by the export cable in a certain period of time [GWh].

2.3. Model computation

All model calculations are computed in Python, a high-level programming language (last access: September 2023). Firstly, the wind-, wave- and solar resources are loaded into the model and the per-source output is computed based on renewable distribution constrained by the spatial park design, using the WaveStar power matrix, and Equations (2) and (3). The per-source- and total park output are then used to calculate the complementary parameters such as PPC (Equation (4)), CoV (Equation (5)), and other relevant aspects for quantifying the synergy of offshore renewables, such as energy density, CF (Equation (6)), and number of hours where park output is below baseload.

3. Results

3.1. Multi-source park output

The per-source- and total-modelled output is depicted in Fig. 2. Fig. 2a shows the total output for the entire considered time frame and portrays the yearly variability in energy generation. The total installed capacity of TNW increases to ~1811 MW, where wind, PV, and wave individually contribute: ~756-, ~1000-, and ~55 MW, respectively. For TNW, the multi-source park output yield [GWh] increases on average by 22% and as this is produced within the same area, the energy density has increased by the same percentage. The coefficient of variation of output decreases 13%, from 0.712 in a wind-farm-only scenario to 0.618 for a multi-source park, indicating more stable output. Fig. 2b portrays the multi-source park output for the year 2015. This year has been chosen as it is most intact in terms of input wind data. Seasonality is apparent, with higher output in the summer due to enhanced PV contribution resulting from increased incoming irradiance. Moreover, both the wave- and wind resources are larger in winter, due to seasonal variability in wind speed [69]. Subsequently, the seasonal variability in the studied time frame between winter and summer is computed as they serve as an envelope in terms of extremes for both autumn and spring. In the winter, the wind output

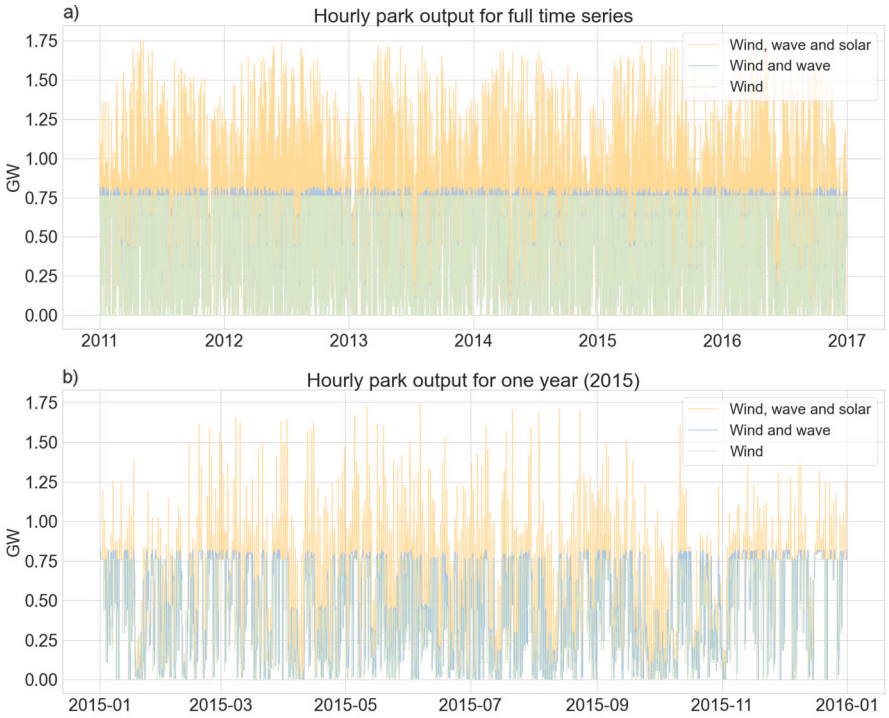

Fig. 2. a) Five-year hourly modelled multi-source TNW electricity output for wind (light green), wind and wave (light blue), and wind, wave, and PV (light orange). b) Hourly modelled multi-source TNW electricity output in 2015 for wind (light green), wind and wave (light blue), and wind, wave, and PV (light orange).

yield is 36.3% more than in the summer, with the CoV increasing from 0.57 in the winter to 0.84 in the summer. For a multi-source park, the difference winter-summer difference in output is 8.4%, with CoV decreasing from 0.69 in summer to 0.54 in winter.
Currently, Tennet is using 700 MW offshore cables but 2000 MW offshore grid connections are being developed to realize the electricity transport from expanding offshore wind farms [70]. The potential curtailment of the multi-source park has been determined for three scenarios: 1) using one 700 MW offshore cable, 2) using a 1000 MW offshore export cable and 3) using two 700 MW offshore cables for a combined capacity of 1400 MW. Fig. 3a depicts the multi-source monthly non-curtailed electricity produced by TNW for these three scenarios. The average yearly non-curtailed production is 4222 GWh, 4802 GWh, and 4946 GWh, respectively, increasing the amount of non-curtailed electricity produced by 17.4%, 27.4%, and 29.5%, depending on the export cable. The average yearly curtailment is 739 GWh, 159 GWh, and 15.4 GWh, respectively.
Fig. 3b shows the load duration curve of the CF scaled to the three different considered export cables. Please note that the input for wind in the model is rounded to zero decimals, causing the 'steps' in the curves of Fig. 3b. For the 700 MW export cable, the multi-source park produces the maximum (or more) cable capacity ~58% of the time and decreases for larger export cables as the number of hours in which the cable capacity is reached declines. An optimized configuration with respect to the export cable in terms of non-curtailed electricity produced and grid stability would be to have the area beneath the load duration curve as large as possible while keeping the amount of curtailed electricity minimal. Fig. 3c depicts the multi-source- and wind-only- average yearly capacity factor for a 700 MW export cable. The capacity factor increases by 19%, from 55% to 74%.

3.2. Reliability and smoothness

To assess the reliability of diverse offshore multi-source energy farms, the statistical complementarity between the renewables and hours and consecutive periods with park output below baseload are computed, as well as the previously presented CoV and CF. These parameters provide insight into how multi-source energy farms can provide an increased stable output for more hours and longer consecutive periods of time, thereby complying better with baseload demand and dampening the need for backup plants in the future.

3.2.1. Statistical correlation

Table 2 shows the average yearly- and seasonal PCC between the considered offshore renewables for different time series frequencies in the studied period.
For all yearly- and seasonal PCC, decreasing the time series frequency results in a stronger correlation between the studied offshore renewables. This happens because reducing the frequency filters out the fine details in the time series. It is most pronounced for offshore PV, where the hourly frequency shows very weak correlations due to the day-night cycle. By decreasing the time series

Fig. 3. a) Monthly non-curtailed electricity produced based on three different export cables 700 MW (blue), 1000 MW (orange), and 2 x 700 MW (green). b) Load duration curve for three different export cables: 700 MW (blue), 1000 MW (orange), and 2 x 700 MW (green). c) Average capacity factor for multi-source (orange) and wind (green) for a 700 MW export cable. The black error bars show the standard deviation of the timeseries.

frequency, this cycle becomes less apparent in the signal. Appendix B shows the offshore PV output for one month using different time series frequencies, demonstrating this data smoothing with reducing time series frequencies.

Wind and wave primarily share a weak to moderate positive PCC in all seasons for different time series frequencies, except autumn with weekly frequency resolution. This implies that these resources are statistically non-complementary to each other, due to the relatively small fetch available in the North Sea, causing the incoming waves to be coupled directly to the local winds and the incoming wave field to be, mostly, free of swell. For an hourly time series frequency, the correlation seems to be smallest in the winter, suggesting that waves are generated less locally, compared to the other seasons.

PV is statistically weak to moderately complementary in all seasons to both wind- and wave energy. This implies that there is a decoupling between the incoming irradiance and the other two offshore resources. The correlations tend to be highest in summer and autumn.

Table 2
Yearly- and seasonal PCC between the different considered offshore renewables for different time series frequency. Negative values imply complementarity and positive values suggest synergy. Higher values within the (|1|,0) range indicate a stronger correlation, low values suggest a weak correlation.

	Annual	Winter	Spring	Summer	Autumn
Wind - Wave					
Hourly	0.27	0.08	0.36	0.33	0.26
Daily	0.39	0.15	0.47	0.47	0.42
Weekly	0.43	-0.12	0.37	0.57	0.54
Wind - Solar					
Hourly	-0.12	-0.04	-0.08	-0.08	-0.09
Daily	-0.31	-0.12	-0.23	-0.23	-0.23
Weekly	-0.48	-0.20	-0.22	-0.27	-0.48
Wave - Solar					
Hourly	-0.04	0.03	-0.07	-0.02	-0.03
Daily	-0.15	0.11	-0.20	-0.18	-0.11
Weekly	-0.23	0.20	0.19	-0.38	-0.28

3.2.2. Virtual base load operation

When the park output is low, only a small percentage of the total capacity of electricity runs through the offshore export cable. This will be further referred to as the virtual base load operation of the offshore cable and serves as a proxy for the reliability of the energy system. For the case study, the considered threshold value for cable virtual base load operation is 140 MW. An important consideration is to determine the length of periods where the output is below the threshold. Long time intervals with low park output are economically undesirable and further, push the need for energy storage systems to comply with the base load and timely energy demands.

Fig. 4a depicts the frequency of occurrence (y-axis, logarithmic) for which a certain period of continuous hours (x-axis) is below a 140 MW export cable utilization threshold (20% of its capacity). It compares a multi-source and wind-only scenario of TNW, with an equal amount of yearly GWh produced. The wind-only output has been upscaled to match the yearly generation of the multi-source park, such that the results in Figs. 4a and 4b are not influenced by the increased capacity of the multi-source park and can be compared directly. Integrating multiple offshore renewables, redistributes the longer periods of output below the threshold observed for the wind farm, to periods with a smaller length of time, visually shifting the graph leftwards. Specifically, a significant decrease in periods longer than 24 hours ($P > 24$ h) is observed (Fig. 4b, y-axis non-logarithmic). In total, the decrease in hours below the threshold based on the Riemann sum is 17.1% and for $P > 24$ h the decrease is 86.5%.

4. Discussion

In this section, we discuss the implications of the presented results on the two challenges identified in the introduction. Note that to accurately model the potential multi-source case for a certain offshore park, a detailed park analysis including a complete spatial design is needed. This includes a spatial plan, considering safety zones, exclusion zones, spacing, and cabling. Though being available for existing wind farms, the exact spatial design is often unresolved for future planned offshore wind farms. The spatial plan presented for TNW is based on a proposed park design and therefore not definite. Moreover, the required spacing and mooring restrictions for offshore PV and wave are yet to be determined. For the spatial park design in this study, a conservative spacing of 250 m is assumed for both offshore PV and WECs. If further tests prove that the PV floaters can be larger and the spacing between floaters and WECS can decrease, the installed capacity inside the park could significantly increase.

With the demonstration and commercialization of various WECs- and floating PV types, future work could compare scenarios that include different WEC- and floating PV technologies. Moreover, the results presented in the case study are an approximation of the total multi-source potential based on previously conducted layouts for an optimized wind park at this location. Follow-up work could further focus on presenting a multi-source offshore energy park that optimizes the business case.

4.1. Power predictability and smoothness

Overall, the yearly power smoothness increases by 13%, indicating that the total park output is more predictable which can lead to enhanced grid balancing and better baseload compliance. The increase in smoothness is more pronounced seasonally, as individual renewables inhibit seasonal variability, especially wind, and PV which share opposite seasonality in terms of maximum output. This strongly balances the multi-source park output on and its smoothness on a seasonal timescale.

Figs. 4a and 4b show that adding other renewable sources like PV and wave reduces the periods with lower baseload production that are longer than one day. The electricity market is organized daily, with intraday and day-ahead markets. In the time period of a single day batteries can play an important role in shifting off-peak supply towards peak supply and overcoming periods with below

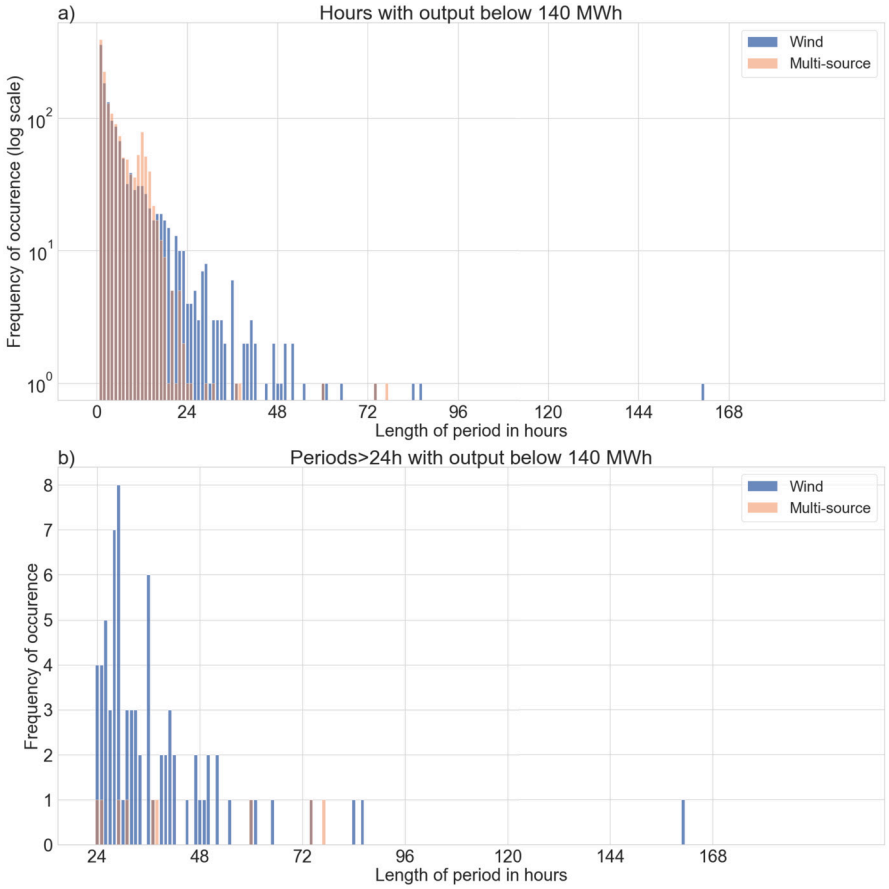

Fig. 4. a) Occurrence (y-axis on a logarithmic scale) of hours (x-axis) with an output below 140 MWh for TNW as a multi-source park (orange) and wind farm (blue). b) Occurrence (y-axis) of periods longer than 24 hours (x-axis) with an output below 140 MWh for TNW as a multi-source park (orange) and wind farm (blue).

base load production of multi-source parks [71]. This can be achieved either with offshore or onshore batteries. Offshore batteries could be mounted on platforms connected to the wind turbine towers or on separate jacket platforms near the substation. With offshore batteries, the advantage is that curtailment due to export cable capacity restrictions can be reduced. On the other hand, onshore batteries have the advantage of allowing the trading of electricity from more than one source. However, there are several other options to shift peak demand to off-peak demand or to overcome intraday periods with lower than baseload production from the multi-source park [72–77].

The periods longer than one day where the TNW multi-source park production is lower than the base load are rather scarce (see Fig. 4b). Electricity can be produced by peaking power plants using gas turbines for example [78]. Since the periods with sub-baseload production are few in number and duration, investment costs (capital costs) could well be leading over fuel costs and plant efficiency (operational costs). These backup power plants are also necessary to add security of supply to the system in case of emergencies.

The Dutch government has set a target of 70 GW of offshore wind power in 2050 [79]. No announcement has been made yet about the target for PV in 2050, but a comparable capacity of PV power will be necessary to balance between winter (more wind, less PV) and summer (more PV, less wind). Preliminary calculations show that with 70 GW offshore wind and a comparable capacity (offshore) PV, around 20% of the export cable capacity of these multi-source energy parks could be sufficient to cover the Dutch average electricity demand [80] of around 25 GW for around 90% of the time. The surplus production of the multi-source parks could be used for offshore hydrogen production units connected to an export pipeline to the coast. It is advisable that these parks are also connected to the coast with a partial load export cable, to support the electricity supply at low wind, wave, and solar conditions, when electricity prices are high. This can be important for the future offshore energy hubs and energy islands that are envisioned by several North Sea coastal countries (Germany, Netherlands, Belgium, and Denmark) [81].

4.2. Energy density

On average, the extracted energy density in the multi-source scenario increases by 22%. In the North Sea, the energy density that offshore wind turbines can accommodate in the North Sea is 2-4 MW/km^2 [2,15]. Assuming the calculated capacity factor of 55%

for offshore wind, at least 67-134 km^2 of marine space would needed for additional wind turbines to produce the same yearly output as the multi-source park. Moreover, if offshore PV and WECs are not to be integrated within wind farms, a minimum of 28 km^2 is necessary to accommodate these renewables as non-co-located parks.

5. Conclusion

Renewable energy targets set by the European Union have led to a rapid build-out of offshore wind in the North Sea. With marine space getting increasingly sparse, the current- and projected upscaling of offshore wind will increase the pressure on chemical-, biological, and physical aspects of the marine ecosystem. Additionally, if North Sea countries are primarily relying on wind energy as their dominating intermittent source, the dependence on cost-efficient large-scale storage systems and fossil fuel-powered backup plants for grid balancing will be essential. This paper presents a novel concept that combines three offshore renewable energy sources, wave-, offshore wind- and offshore PV, into a multi-source offshore energy park with the potential to transform the future energy system.

The yearly electricity output and extracted energy density of such a multi-source park increase by 22%, by utilizing the same amount of marine space and a majority of the existing infrastructure, ultimately, reducing the pressure on the overall marine ecosystem and other stakeholders. The addition of wave- and solar as different intermittent sources than wind shows a strong improvement in grid reliability and security. The multi-source park's energy output is smoother as its coefficient of variation decreases by a yearly average of 13%, the capacity factor with respect to the export cable increases by 19%, and hours in prolonged periods ($P > 24$ h) with production lower than 140 MW (20% of the export cable capacity) decreases by 86.5%. This implies that the park output is less volatile, thereby better balancing the grid and the strong decrease in periods with low output allows it to be more easily balanced in the future by storage systems, reducing the need to rely on non-renewable backup plants.

These findings have been applied to a planned offshore wind farm area in the Netherlands without optimizing the previous work proposed intra-array grid. The result is that this use-case is not optimized for being a multi-source park in terms of renewable energy distribution, but still shows strong benefits for adding wave and solar to it. The real case scenario of this offshore wind farm being built further increases the value for current decision-makers, while being a blueprint for future multi-source parks around the world.

Data and code availability

The exact wind- and solar resource input data is available at https://www.knmi.nl/nederland-nu/klimatologie/uurgegevens and https://re.jrc.ec.europa.eu/pvg_tools/en/, respectively. The wave input data is owned by Delft University of Technology and can therefore only be requested from them directly. Alternatively, the open-source RESOURCECODE database can be used for wave data, available at https://resourcecode.ifremer.fr/. While the equations stated in the paper provide the exact method to replicate the results presented in this paper, the Python code used can be made available on request.

CRediT authorship contribution statement

Hinne F. van der Zant: Writing – review & editing, Writing – original draft, Visualization, Validation, Software, Methodology, Investigation, Formal analysis, Data curation, Conceptualization. **Anne-Caroline Pillet:** Software, Methodology. **Anton Schaap:** Writing – review & editing, Writing – original draft, Supervision, Methodology. **Simon J. Stark:** Writing – review & editing, Supervision. **Timothy A. de Weijer:** Writing – original draft. **Aida A. Cahyaningwidi:** Writing – review & editing, Writing – original draft. **Benjamin A.E. Lehner:** Writing – review & editing, Writing – original draft, Supervision, Methodology, Formal analysis.

Declaration of competing interest

The authors declare that they have no known competing financial interests or personal relationships that could have appeared to influence the work reported in this paper.

Acknowledgement

The authors of this paper would acknowledge George Lavidas for providing the wave data used in this study as part of the TKI Dutch-WATERS project. The paper was further assisted by the Interreg2Seas ENCORE (ENergising COastal Regions with Offshore Renewable Energy) and the EU-SCORES project which has received funding from the Europeans Union Horizon 2020 research & innovation programme under grant agreement number 101036457.

Appendix A. Yearly- and seasonal Kendall correlation coefficients

	Annual	Winter	Spring	Summer	Autumn
Wind - Wave					
Hourly	0.46	0.43	0.39	0.36	0.48
Daily	0.51	0.44	0.45	0.42	0.54
Weekly	0.59	0.46	0.45	0.54	0.67
Wind - Solar					
Hourly	-0.08	-0.02	-0.04	-0.03	-0.05
Daily	-0.21	-0.06	-0.15	-0.16	-0.13
Weekly	-0.34	-0.16	-0.20	-0.16	-0.32
Wave - Solar					
Hourly	-0.10	-0.03	-0.03	-0.01	-0.05
Daily	-0.28	-0.12	-0.16	-0.17	-0.18
Weekly	-0.44	-0.16	-0.12	-0.32	-0.36

Yearly- and seasonal Kendall correlation coefficients. The Pearson correlation (Fig. 3a) is statistically more robust, compared to Kendall, but requires linear relation between the input variables, unlike Kendall. If the Kendall coefficient strongly differs from the Pearson coefficient, the considered offshore renewables for that time series frequency likely share a non-linear relation, rendering the Pearson coefficient to be less accurate. In that case, the Kendall coefficient will provide a better statistical correlation approximation.

Appendix B. Monthly PV output for different time series frequencies

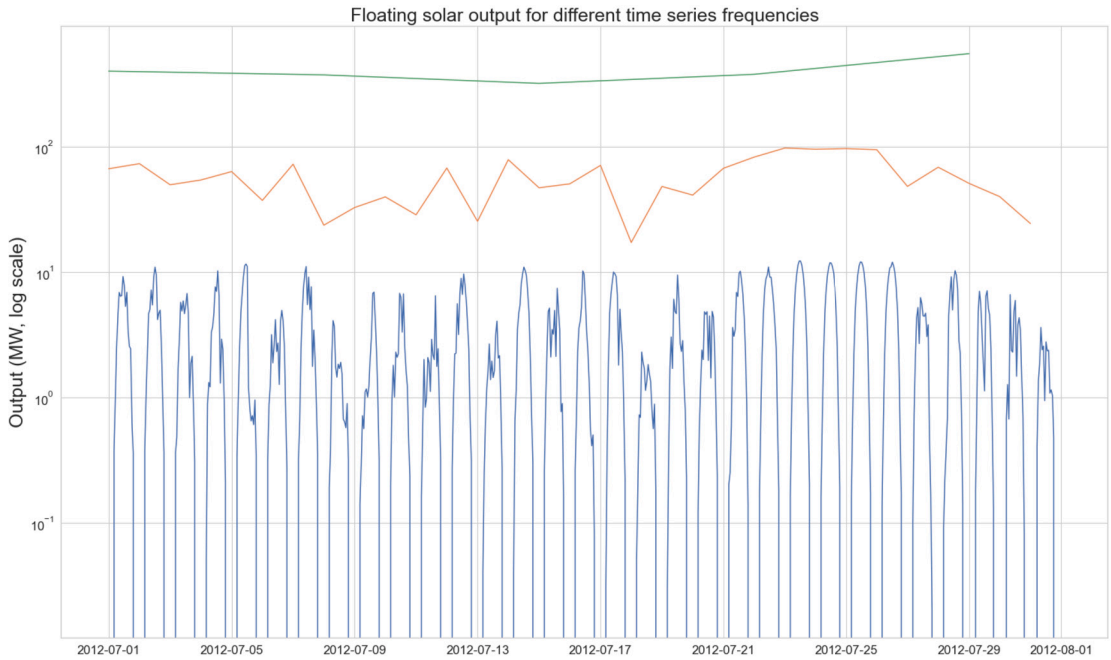

Monthly PV output for different time series frequencies. When decreasing the frequency, the fine signal in the data series is lost. For PV, this filters out the day-night cycle. This makes the correlation coefficient for daily time series frequencies more comprehensive, as when using an hourly frequency, the correlation will be low as there is per definition no correlation with other resources during the night.

References

[1] European Commission, Communication from the commission to the European Parliament, the European Council, the Council, the European Economic and Social Committee and the Committee of the Regions, https://eur-lex.europa.eu/legal-content/EN/TXT/?uri=COM%3A2022%3A230%3AFIN&qid=1653033742483, 2022.

[2] Floris Taminiau, Bob van der Zwaan, The physical potential for Dutch offshore wind energy, in: Available at SSRN 4109358, 2022, https://doi.org/10.21926/jept.2204032.

[3] Wind Europe, Offshore Wind in Europe, key trends and statistics 2019, Tech. rep., Wind Europe, 2020, https://windeurope.org/about-wind/statistics/offshore/european-offshore-wind-industry-key-trends-statistics-2019/.

[4] Ute Daewel, et al., Offshore wind farms are projected to impact primary production and bottom water deoxygenation in the North Sea, Commun. Earth Environ. 3 (1) (2022) 292, https://doi.org/10.1038/s43247-022-00625-0.

[5] Wind Europe, Wind energy in Europe - 2021 Statistics and the outlook for 2022–2026, Tech. rep., Wind Europe, 2021, https://windeurope.org/intelligence-platform/product/wind-energy-in-europe-2022-statistics-and-the-outlook-for-2023-2027/.

[6] Wind Europe, Our Energy Our Future - How offshore wind will help Europe go carbon-neutral, Tech. rep., Wind Europe, 2019, https://windeurope.org/wp-content/uploads/files/about-wind/reports/WindEurope-Our-Energy-Our-Future.pdf.

[7] Lena Bergström, et al., Effects of offshore wind farms on marine wildlife—a generalized impact assessment, Environ. Res. Lett. 9 (3) (2014) 034012, https://doi.org/10.1088/1748-9326/9/3/034012.

[8] Naveed Akhtar, et al., Accelerating deployment of offshore wind energy alter wind climate and reduce future power generation potentials, Sci. Rep. 11 (1) (2021) 11826, https://doi.org/10.1038/s41598-021-91283-3.

[9] Nils Christiansen, et al., Emergence of large-scale hydrodynamic structures due to atmospheric offshore wind farm wakes, Front. Mar. Sci. 9 (2022) 64, https://doi.org/10.3389/fmars.2022.818501.

[10] Elke Ludewig, Influence of offshore wind farms on atmosphere and ocean dynamics, PhD thesis, Staats-und Universitätsbibliothek Hamburg Carl von Ossietzky, 2013, https://ediss.sub.uni-hamburg.de/handle/ediss/5270?mode=full.

[11] Jens Floeter, et al., Pelagic effects of offshore wind farm foundations in the stratified North Sea, Prog. Oceanogr. 156 (2017) 154–173, https://doi.org/10.1016/j.pocean.2017.07.003.

[12] Anna Reese, et al., Characterization of alloying components in galvanic anodes as potential environmental tracers for heavy metal emissions from offshore wind structures, Chemosphere 257 (2020) 127182, https://doi.org/10.1016/j.chemosphere.2020.127182.

[13] Jeffrey R. Carpenter, et al., Potential impacts of offshore wind farms on North Sea stratification, PLoS ONE 11 (8) (2016) e0160830, https://doi.org/10.1371/journal.pone.0160830.

[14] R.M. Forster, The effect of monopile-induced turbulence on local suspended sediment pattern around UK wind farms. An IECS report to the Crown Estate, Tech. rep., Institute of Estuarine and Coastal Studies, 2018, https://ore.catapult.org.uk/wp-content/uploads/2018/12/The-Effect-of-Monopile-Induced-Turbulence-on-Local-Suspended-Sediment-Pattern-around-UK-Wind-Farms.pdf.

[15] Laura Florentina Gusatu, et al., A spatial analysis of the potentials for offshore wind farm locations in the North Sea region: challenges and opportunities, ISPRS Int.l J. Geo-Inf. 9 (2) (2020) 96, https://doi.org/10.3390/ijgi9020096.

[16] Samuel C. Johnson, et al., Evaluating rotational inertia as a component of grid reliability with high penetrations of variable renewable energy, Energy 180 (2019) 258–271, https://doi.org/10.1016/j.energy.2019.04.216.

[17] Ali Q. Al-Shetwi, et al., Grid-connected renewable energy sources: review of the recent integration requirements and control methods, J. Clean. Prod. 253 (2020) 119831, https://doi.org/10.1016/j.jclepro.2019.119831.

[18] Francesco Fusco, Gary Nolan, John V. Ringwood, Variability reduction through optimal combination of wind/wave resources – an Irish case study, Energy (ISSN 0360-5442) 35 (2010) 314–325, https://doi.org/10.1016/j.energy.2009.09.023.

[19] Eric D. Stoutenburg, Nicholas Jenkins, Mark Z. Jacobson, Power output variations of co-located offshore wind turbines and wave energy converters in California, Renew. Energy (ISSN 0960-1481) 35 (2010) 2781–2791, https://doi.org/10.1016/j.renene.2010.04.033.

[20] S. Astariz, G. Iglesias, Output power smoothing and reduced downtime period by combined wind and wave energy farms, Energy (ISSN 0360-5442) 97 (2016) 69–81, https://doi.org/10.1016/j.energy.2015.12.108.

[21] Francisco Haces-Fernandez, Hua Li, David Ramirez, A layout optimization method based on wave wake preprocessing concept for wave-wind hybrid energy farms, Energy Convers. Manag. (ISSN 0196-8904) 244 (2021) 114469, https://doi.org/10.1016/j.enconman.2021.114469.

[22] Roan A. Gideon, Elie Bou-Zeid, Collocating offshore wind and wave generators to reduce power output variability: a multi-site analysis, Renew. Energy (ISSN 0960-1481) 163 (2021) 1548–1559, https://doi.org/10.1016/j.renene.2020.09.047.

[23] Shona Pennock, et al., Temporal complementarity of marine renewables with wind and solar generation: implications for GB system benefits, Appl. Energy 319 (2022) 119276, https://doi.org/10.1016/j.apenergy.2022.119276.

[24] Marcolino Matheus de Souza Nascimento, et al., Offshore wind and solar complementarity in Brazil: a theoretical and technical potential assessment, Energy Convers. Manag. (ISSN 0196-8904) 270 (2022) 116194, https://doi.org/10.1016/j.enconman.2022.116194, https://www.sciencedirect.com/science/article/pii/S0196890422009712.

[25] Takvor H. Soukissian, Flora E. Karathanasi, Dimitrios K. Zaragkas, Exploiting offshore wind and solar resources in the Mediterranean using ERA5 reanalysis data, Energy Convers. Manag. (ISSN 0196-8904) 237 (2021) 114092, https://doi.org/10.1016/j.enconman.2021.114092, https://www.sciencedirect.com/science/article/pii/S0196890421002685.

[26] George Lavidas, Kornelis Blok, Shifting wave energy perceptions: the case for wave energy converter (WEC) feasibility at milder resources, Renew. Energy 170 (2021) 1143–1155, https://doi.org/10.1016/j.renene.2021.02.041.

[27] Flemming Schlütter, Ole Svenstrup Petersen, Lotte Nyborg, Resource mapping of wave energy production in Europe, in: Proceedings of the 11th European Wave and Tidal Energy Conference, 2015, pp. 6–11, https://tethys-engineering.pnnl.gov/sites/default/files/publications/schlutteretal2015.pdf.

[28] Mario López, Noel Rodríguez, Gregorio Iglesias, Combined floating offshore wind and solar PV, J. Mar. Sci. Eng. 8 (8) (2020) 576, https://doi.org/10.3390/jmse8080576.

[29] X. Costoya, et al., Combining offshore wind and solar photovoltaic energy to stabilize energy supply under climate change scenarios: a case study on the western Iberian Peninsula, Renew. Sustain. Energy Rev. (ISSN 1364-0321) 157 (2022) 112037, https://doi.org/10.1016/j.rser.2021.112037, https://www.sciencedirect.com/science/article/pii/S1364032121012995.

[30] Syed Raahat Ara, Santanu Paul, Zakir Hussain Rather, Two-level planning approach to analyze techno-economic feasibility of hybrid offshore wind-solar pv power plants, Sustain. Energy Technol. Assess. (ISSN 2213-1388) 47 (2021) 101509, https://doi.org/10.1016/j.seta.2021.101509, https://www.sciencedirect.com/science/article/pii/S2213138821005208.

[31] S.Z.M. Golroodbari, et al., Pooling the cable: a techno-economic feasibility study of integrating offshore floating photovoltaic solar technology within an offshore wind park, Sol. Energy 219 (2021) 65–74, https://doi.org/10.1016/j.solener.2020.12.062.

[32] S. Astariz, et al., Co-located wind-wave farm synergies (Operation & Maintenance): a case study, Energy Convers. Manag. 91 (2015) 63–75, https://doi.org/10.1016/j.enconman.2014.11.060.

[33] S. Astariz, et al., Co-located wave-wind farms for improved O&M efficiency, Ocean Coast. Manag. 163 (2018) 66–71, https://doi.org/10.1016/j.ocecoaman.2018.04.010.

[34] Jocelyn M. Kluger, Maha N. Haji, Alexander H. Slocum, The power balancing benefits of wave energy converters in offshore wind-wave farms with energy storage, Appl. Energy 331 (2023) 120389, https://doi.org/10.1016/j.apenergy.2022.120389.

[35] C. Pérez-Collazo, D. Greaves, G. Iglesias, A review of combined wave and offshore wind energy, Renew. Sustain. Energy Rev. (ISSN 1364-0321) 42 (2015) 141–153, https://doi.org/10.1016/j.rser.2014.09.032.

[36] Arianna Azzellino, et al., Optimal siting of offshore wind-power combined with wave energy through a marine spatial planning approach, Int. J. Mar. Energy (ISSN 2214-1669) 3–4 (2013) e11–e25, https://doi.org/10.1016/j.ijome.2013.11.008.

[37] S. Astariz, et al., Towards the optimal design of a co-located wind-wave farm, Energy (ISSN 0360-5442) 84 (2015) 15–24, https://doi.org/10.1016/j.energy.2015.01.114.

[38] S. Astariz, G. Iglesias, Selecting optimum locations for co-located wave and wind energy farms. Part I: the co-location feasibility index, Energy Convers. Manag. (ISSN 0196-8904) 122 (2016) 589–598, https://doi.org/10.1016/j.enconman.2016.05.079, https://www.sciencedirect.com/science/article/pii/S0196890416304642.
[39] S. Astariz, G. Iglesias, Selecting optimum locations for co-located wave and wind energy farms. Part II: a case study, Energy Convers. Manag. (ISSN 0196-8904) 122 (2016) 599–608, https://doi.org/10.1016/j.enconman.2016.05.078, https://www.sciencedirect.com/science/article/pii/S0196890416304630.
[40] S. Astariz, et al., Hybrid wave and offshore wind farms: a comparative case study of co-located layouts, Int. J. Mar. Energy (ISSN 2214-1669) 15 (2016) 2–16, https://doi.org/10.1016/j.ijome.2016.04.016.
[41] S. Astariz, G. Iglesias, Co-located wind and wave energy farms: uniformly distributed arrays, Energy (ISSN 0360-5442) 113 (2016) 497–508, https://doi.org/10.1016/j.energy.2016.07.069.
[42] Weixing Chen, et al., W2P: a high-power integrated generation unit for offshore wind power and ocean wave energy, Ocean Eng. (ISSN 0029-8018) 128 (2016) 41–47, https://doi.org/10.1016/j.oceaneng.2016.10.017.
[43] George Lavidas, Selection index for wave energy deployments (SIWED): a near-deterministic index for wave energy converters, Energy 196 (2020) 117131, https://doi.org/10.1016/j.energy.2020.117131.
[44] Pim Rooijmans Ben de Sonneville, Eric Weekamp, Haydar Hussin, Erik Holtslag, Study into Levelized Cost of Energy of Variants for Wind Farm Site Boundaries of Hollandse Kust (West), Ten Noorden van de Waddeneilanden and IJmuiden Ver, BLIX Consultancy BV & Partners, 2018, https://www.rvo.nl/sites/default/files/2018/12/20181114_BLIX_RVO_LCOE_HKW_TNW_IJV_F.pdf.
[45] Joost Sissingh, Handreiking gebiedspaspoort Borssele, Tech. rep. Pondera consult, 2020.
[46] Lyndon Greedy, Tino Schlemmer, 66 kV Systems for Offshore Wind Farms, Tech. rep. DNV GL Energy, 2015, https://silo.tips/download/tennet-nl-offshore-wind-farm-transmission-systems.
[47] Inkscape, Open source vector editing software, https://inkscape.org/, 2023. (Accessed October 2023).
[48] Charlotte Beels, et al., Wave energy resource in the North Sea, in: EWTEC 2007-7th European Wave and Tidal Energy Conference, 2007.
[49] Pim Rooijmans Ben de Sonneville, Eric Weekamp, Haydar Hussin, Erik Holtslag, Wake effects of three modified versions of TNW variant 2, Tech. rep., BLIX Consultancy BV & Partners, 2018.
[50] 4Coffshore, Global offshore renewable map, https://map4coffshore.com/offshorewind/. (Accessed October 2023).
[51] I. van der Werf, Slow Mill 3D Farm proeven, Tech. rep. Deltaris, 2019, https://www.deltares.nl/en/expertise/areas-of-expertise/energy-transition/wave-energy-supplementing-the-energy-transition.
[52] Morten Kramer, Laurent Marquis, Peter Frigaard, Performance evaluation of the wavestar prototype, in: 9th Ewtec 2011: Proceedings of the 9th European Wave and Tidal Conference, Southampton, UK, 5th-9th September 2011, University of Southampton, 2011, https://vbn.aau.dk/en/publications/performance-evaluation-of-the-wavestar-prototype-2, 2011.
[53] Wave Star A/S, Wavestar prototype at Roshage, Performance data for ForskVE project no 2009-1-10305 phase 1 & 2, January 2013, Tech. rep., Wave Star A/S, 2013, https://tethys.pnnl.gov/sites/default/files/publications/Wavestar-Performance-Data-2013.pdf.
[54] N. Booij, L.H. Holthuijsen, R.C. Ris, The “SWAN” wave model for shallow water, Coastal Eng. Proc. 25 (1996), https://doi.org/10.1061/9780784402429.053.
[55] N.R.R.C. Booij, Roeland C. Ris, Leo H. Holthuijsen, A third-generation wave model for coastal regions: 1. Model description and validation, J. Geophys. Res., Oceans 104 (C4) (1999) 7649–7666, https://doi.org/10.1029/98JC02622.
[56] R.C. Ris, L.H. Holthuijsen, N. Booij, A third-generation wave model for coastal regions: 2. Verification, J. Geophys. Res., Oceans 104 (C4) (1999) 7667–7681, https://doi.org/10.1029/1998JC900123.
[57] D. Silva, C. Guedes Soares, Validation with satellite data of SWAN model for wave conditions at the Madeira archipelago, in: Developments in Maritime Technology and Engineering, CRC Press, 2021, pp. 665–672.
[58] Eugen Rusu, Liliana Rusu, An evaluation of the wave energy resources in the proximity of the wind farms operating in the North Sea, Energy Rep. 7 (2021) 19–27, https://doi.org/10.1016/j.egyr.2021.05.058.
[59] Shahram Derakhshan, Mahdi Moghimi, Hadi Motawej, Development of a mathematical model to design an offshore wind and wave hybrid energy system, Energy Equip. Syst. 6 (2) (2018) 181–200, https://doi.org/10.22059/ees.2018.31536.
[60] Anik Goswami, Pradip Kumar Sadhu, Degradation analysis and the impacts on feasibility study of floating solar photovoltaic systems, Sustain. Energy Grids Netw. 26 (2021) 100425, https://doi.org/10.1016/j.segan.2020.100425.
[61] Thomas Huld, Richard Müller, Attilio Gambardella, A new solar radiation database for estimating PV performance in Europe and Africa, Sol. Energy 86 (6) (2012) 1803–1815, https://doi.org/10.1016/j.solener.2012.03.006.
[62] GE Renewable Energy, Haliade-X offshore wind turbine, https://www.ge.com/renewableenergy/wind-energy/offshore-wind/haliade-x-offshore-turbine, 2022.
[63] Royal Netherlands Meteorological Institute (KNMI), Hourly data of the weather in the Netherlands, https://www.knmi.nl/nederland-nu/klimatologie/uurgegevens. (Accessed 9 November 2023).
[64] H. Tennekes, The logarithmic wind profile, J. Atmos. Sci. 30 (2) (1973) 234–238, https://doi.org/10.1175/1520-0469(1973)030<0234:TLWP>2.0.CO;2.
[65] David Sharpe, Wind Energy Handbook, John Wiley & Sons, Ltd, 2001.
[66] Yves-Marie Saint-Drenan, et al., A parametric model for wind turbine power curves incorporating environmental conditions, Renew. Energy 157 (2020) 754–768, https://doi.org/10.1016/j.renene.2020.04.123.
[67] Takvor H. Soukissian, Flora E. Karathanasi, Dimitrios K. Zaragkas, Exploiting offshore wind and solar resources in the Mediterranean using ERA5 reanalysis data, Energy Convers. Manag. 237 (2021) 114092, https://doi.org/10.1016/j.enconman.2021.114092.
[68] Mauricio P. Cantão, et al., Evaluation of hydro-wind complementarity in the Brazilian territory by means of correlation maps, Renew. Energy 101 (2017) 1215–1225, https://doi.org/10.1016/j.renene.2016.10.012.
[69] J.P. Coelingh, A.J.M. Van Wijk, A.A.M. Holtslag, Analysis of wind speed observations over the North Sea, J. Wind Eng. Ind. Aerodyn. 61 (1) (1996) 51–69, https://doi.org/10.1016/0167-6105(96)00043-8.
[70] TenneT, Tennet develops innovative submarine cables with suppliers, https://www.tennet.eu/tinyurl-storage/detail/tennet-develops-innovative-submarine-cable-with-suppliers/, 2020.
[71] Tom Feehally, et al., Battery energy storage systems for the electricity grid: UK research facilities, https://doi.org/10.1049/cp.2016.0257, 2016.
[72] Ram Deivanayagam, Vehicle-to-grid technology: concept, status, and challenges, J. Undergrad. Res. Univ. Ill. Chicago 10 (1) (2017) 1, https://doi.org/10.5210/jur.v10i1.8013.
[73] Thomas Wenning Paulomi Nandy, Alexandra Botts, Demand Response in Industrial Facilities: Peak Electricity Demand, Tech. rep., U.S. Department of Energy, 2022.
[74] Elisa Guelpa, Vittorio Verda, Thermal energy storage in district heating and cooling systems: a review, Appl. Energy 252 (2019) 113474, https://doi.org/10.1016/j.apenergy.2019.113474.
[75] Claire Bergaentzlé, Cédric Clastres, Demand side management in an integrated electricity market: what are the impacts on generation and environmental concerns?, in: 2013 10th International Conference on the European Energy Market (EEM), IEEE, 2013, pp. 1–8.
[76] Ilya Chernyakhovskiy, et al., Forecasting Wind and Solar Generation: Improving System Operations, Greening the Grid. Tech. rep. National Renewable Energy Lab., NREL, Golden, CO (United States), 2016, https://www.osti.gov/biblio/1236672.
[77] IRENA and KEEI, Renewable energy and electricity interconnections for a sustainable Northeast Asia, Tech. rep., International Renewable Energy Agency, Abu Dhabi, 2021, https://www.irena.org/Publications/2021/May/Renewable-Energy-and-Electricity-Interconnections-for-a-Sustainable-Northeast-Asia.

[78] Siemens, Industrial gas turbines: the perfect complement for renewables-plus-storage, https://assets.siemens-energy.com/siemens/assets/api/uuid:701e53fc-9cc1-4ebc-957d-ff4d9c5c8efc/flexible-generation-teit-02092021.pdf, 2021.
[79] Ministerie van Algemene Zaken. Duurzame Energie, https://www.rijksoverheid.nl/onderwerpen/duurzame-energie, 2022.
[80] NetbeheerNL, The Energy System of the Future, Tech. rep., Netbeheer, Nederland, 2021, https://www.netbeheernederland.nl/_upload/files/NetbeheerNL_Rapport-Samenvatting-ENG_A4_FC.pdf.
[81] Ministerie van Algemene Zaken, Nederland Maakt ambitie wind op Zee Bekend: 70 gigawatt in 2050, https://www.rijksoverheid.nl/actueel/nieuws/2022/09/16/nederland-maakt-ambitie-wind-op-zee-bekend-70-gigawatt-in-2050, Sept. 2022.